PROCEEDINGS, Twenty-Eighth Workshop on Geothermal Reservoir Engineering
Stanford University, Stanford, California, January 27-29, 2003
SGP-TR-173

CHARACTERIZATION OF FRACTURED RESERVOIRS USING CONTINUOUS SELF-POTENTIAL MEASUREMENTS

Tsuneo Ishido and John W. Pritchett*

Geological Survey of Japan, AIST
Central 7
Tsukuba, 305-8567, Japan
e-mail: ishido-t@aist.go.jp

*Science Applications International Corp.
10260 Campus Point Drive
San Diego, CA92121

ABSTRACT

We have extended our "EKP-postprocessor" (Ishido and Pritchett, 1996) to calculate electrokinetic potentials in fractured geothermal reservoirs that are represented computationally as "MINC" double-porosity media. In such reservoir descriptions, global mass exchange between adjacent macroscopic computational grid blocks takes place mainly through the "fracture zone". Inter-block flow through the "matrix region" is relatively unimportant and is usually neglected in most MINC treatments. But this approximation is inappropriate when calculating the global "drag current" caused by electric charges moving with the flowing fluid due to electrokinetic coupling. Since the magnitude of the drag current density is proportional not to the permeability but to the porosity of the medium, the contribution of the drag current through the matrix region to the total global current between adjacent macroscopic grid blocks is not negligible, and in fact usually predominates under steady-state conditions. This property of the drag current brings about much more pronounced differences in the "self-potential transients" between competing "fractured/MINC" and "porous-medium" descriptions of the same reservoir than is the case for pressure transients. Combining continuous pressure and self-potential measurements may therefore provide a means for better characterizing fractured geothermal reservoirs.

INTRODUCTION

Since the 1970's, the SP (self-potential) method has attracted increasing interest in geothermal prospecting and engineering geophysics. Among the various mechanisms which can cause SP in geothermal settings, the most important appear to be electrokinetic (streaming) potentials arising from underground fluid flow caused by hydrothermal activity and topographic effects (e.g. Zohdy et al., 1973; Zablocki, 1976; Corwin and Hoover, 1979; Ishido, 1989). Ishido et al. (1987) also pointed out that production-induced SP changes can be observed via electrokinetic coupling in geothermal areas.

We developed the so-called "EKP-postprocessor" to calculate space/time distributions of electrokinetic potentials resulting from histories of underground conditions (pressure, temperature, vapor saturation, concentration of dissolved species, flowrate, etc.) computed by unsteady multi-dimensional geothermal reservoir simulations (Ishido and Pritchett, 1996). The postprocessor can be applied to "history-matching" of self-potential (SP) data, since changes in SP are mainly caused by electrokinetic effects, especially in the early stages of field exploitation.

Recently, we have extended the EKP-postprocessor to apply it to fractured reservoirs. In this paper, we outline the new features and introduce some results of pressure-transient test simulations. These preliminary results show that downhole SP monitoring is a promising technique for better characterizing fractured reservoirs.

EXTENDING THE EKP-POSTPROCESSOR TO "MINC" MEDIA

Electrokinetic Coupling

The flow of a fluid through a porous medium may generate an electrical potential gradient (called the electrokinetic or streaming potential) along the flow path by the interaction of the moving pore fluid with the electrical double layer at the pore surface. This process is known as electrokinetic coupling. The general relations between the electric current density

I and fluid volume flux **J**, and the electric potential gradient $\nabla\phi$ and pore pressure gradient $\nabla\xi$ forces are

$$\mathbf{I} = - L_{ee} \nabla\phi - L_{ev} \nabla\xi \quad (1)$$

$$\mathbf{J} = - L_{ve} \nabla\phi - L_{vv} \nabla\xi \quad (2)$$

where the L_{ij} are phenomenological coefficients (e.g. Ishido and Mizutani, 1981). The first term on the right-hand side in (1) represents Ohm's law and the second term in (2) represents Darcy's law. The cross-coupling terms (with the L_{ev} and L_{ve} coefficients) represent the electrokinetic effect; $L_{ev} = L_{ve}$ according to Onsagar's reciprocal relations.

Based upon a capillary model, the above coefficients may be written as follows (Ishido and Mizutani, 1981):

$$L_{ev} = -\eta \varepsilon \zeta R_{ev} G/\tau \mu \quad (3)$$

$$L_{ee} = \eta(\sigma + m^{-1}\Sigma_s)/ \tau \quad (4)$$

where:

η = porosity,
ε = liquid-phase dielectric permittivity,
ζ = zeta-potential,
R_{ev} = "electrical relative permeability" for two-phase flow,
G = correction factor which becomes less than unity only if the hydraulic radius is comparable to the thickness of the electrical double layer,
τ = square of tortuosity ($\tau = t^2$),
μ = liquid-phase viscosity,
σ = electrical conductivity of pore fluid,
m = hydraulic radius of pores and/or cracks,
Σ_s = surface condactance.

Eqn. (1) describes the total current density, composed of a drag (convection) current density $\mathbf{I}_{drag}$ caused by charges moved by fluid flow, and a conduction current density $\mathbf{I}_{cond}$ caused by electric conduction; hence,

$$\mathbf{I} = \mathbf{I}_{cond} + \mathbf{I}_{drag} \quad (5)$$

where

$$\mathbf{I}_{cond} = -L_{ee} \nabla\phi$$

$$\mathbf{I}_{drag} = -L_{ev} \nabla\xi$$

In the absence of external current sources, $\nabla\cdot\mathbf{I} = 0$, so from (5):

$$\nabla\cdot\mathbf{I}_{cond} = - \nabla\cdot\mathbf{I}_{drag} \quad (6)$$

Eqn. (6) represents sources of conduction current that are required for the appearance of electric potential.

In a homogeneous region, Eqn. (6) can be written as:

$$\nabla^2\phi = C \nabla^2 \xi \quad (7)$$

where C is called the streaming potential coefficient:

$$C = -L_{ev}/ L_{ee} = \varepsilon \zeta / (\sigma + m^{-1}\Sigma_s)\mu \quad (8)$$

If the pore pressure change occurs within a finite homogeneous volume, the following relation between changes in ϕ (streaming potential) and ξ (pressure) prevails:

$$\Delta\phi = C\Delta\xi \quad (9)$$

EKP-postprocessor

The cross-coupling term in (2) may be safely neglected for typical geologic situations, and Darcy's law alone may be used to model the hydraulic problem; it is not necessary to solve (1) and (2) simultaneously. A "postprocessor" may then be used to calculate the drag current ($\mathbf{I}_{drag}$) from the results of an unsteady thermohydraulic reservoir simulation.

The "EKP-postprocessor" (Ishido and Pritchett, 1996; see also Ishido and Pritchett, 1999) simulates electric potentials caused by subsurface fluid flow by a two-step process. First, it calculates the distribution of L_{ev}, L_{ee} and $\mathbf{I}_{drag}$ from the reservoir-simulation results using the same spatial grid used for the reservoir simulation calculation (called the RSV-grid hereafter). Next, the postprocessor calculates the electric potential (ϕ) distribution by solving the above Poisson equation (6) within a finite-difference grid that is usually much greater in spatial extent than the RSV-grid (hereafter called the SP-grid).

Within that portion of the SP-grid overlapped by the RSV-grid, the distribution of electrical conductivity is obtained directly from RSV-grid values. Elsewhere within the SP-grid, the electrical conductivity distribution is user-specified and time-invariant. Ordinarily, boundary conditions on the potential are: zero normal gradients (Neumann condition) on the ground surface (upper surface) and zero potential (Dirichlet condition) along the bottom and vertical sides of the SP-grid. It is also possible to prescribe zero normal gradients on all exterior surfaces of the SP-grid. Eqn. (6) is solved numerically using a Gauss-Seidel iteration procedure incorporating intermittent automatic optimization of the overrelaxation factor.

The EKP-postprocessor was originally developed as one of the mathematical postprocessors for the "STAR" code (Pritchett, 1995). The reservoir-simulation results required for postprocessor calculations are stored on the so-called "*GEO*" output file. An interface program is now also available to create a "*GEO*" file from the results of "TOUGH2" reservoir simulations.

Streaming Potential in Low-k Rocks

The streaming potential coefficient C (Eqn.8) can be measured in the laboratory as an electric potential difference $\Delta\phi$ induced by a pressure difference ΔP imposed across the two ends of a sample plug. Although the sample plug is usually composed of crushed grains for rock/water systems (see, e.g.

Ishido and Mizutani, 1981), there have been several C measurements for intact rock samples (e.g. Jouniaux and Pozzi, 1995).

Figures 1 and 2 show the temperature and salinity dependence of C and L_{ee} respectively measured for an intact granite sample (Tosha et al., 2003). The magnitude of C is smaller than that measured for a granular sample of the same granite (which is available only for temperatures below 80°C; Ishido and Mizutani, 1981): the magnitude for the granular sample is several times and several tens times larger than that of the intact sample at salt concentrations of 0.01 and 0.001 mol/L respectively. This reduction in |C| is due to significant contribution of the surface conductance to L_{ee} for the intact sample (which has smaller hydraulic radius m; see Eqn. 4).

Figure 3 shows the zeta potential obtained using Eqn. (8) from the data shown in Figures 1 and 2. Since the hydraulic radius, estimated from the permeability of $\sim 10^{-18}$ m^2, is $\sim 10^{-7}$ meter for this sample, (which is an order of magnitude larger than the $\sim 10^{-8}$ m thickness of the electrical double layer for 0.001 mol/L salt concentration), we assumed G=1 in Eqn. 8. This estimated zeta potential magnitude is comparable to that measured for the granular sample (denoted by "G" in Figure 3) and to theoretical predictions (labeled "I&M" in Figure 3). This implies that Eqn. (3), with G=1, can be applied to low-permeability rocks such as the present sample and substantial drag current will be induced in the matrix region of fractured reservoirs as long as the permeability exceeds one microdarcy or so.

Model for Drag Current in MINC Media

The model which we adopt to calculate the drag current density in "MINC" media (Pruess and Narasimhan, 1982) amounts to the following:

$$\mathbf{I_{total}} = \mathbf{I_f} + \mathbf{I_m} \qquad (10)$$

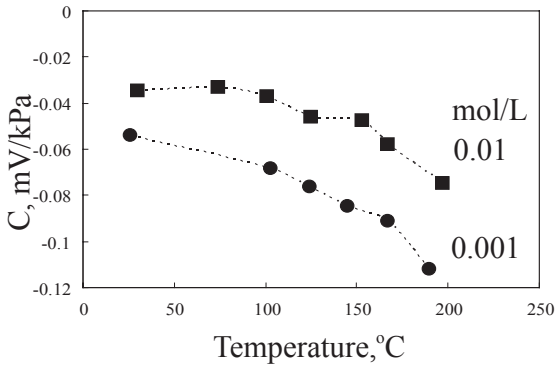

Figure 1. Streaming potential coefficient of Inada granite saturated with 0.001 mol/L (circles) and 0.01 mol/L (squares) KCl solutions. (Figures 1 to 3 are modified from Tosha et al., 2003)

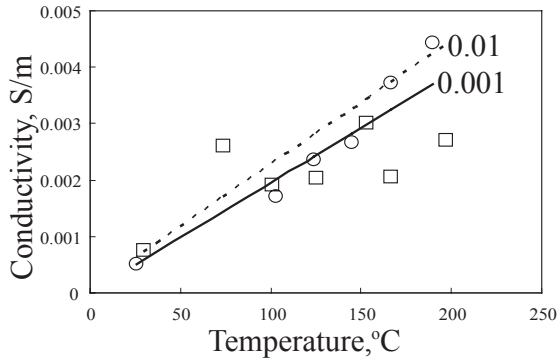

Figure 2. Electrical conductivity L_{ee} of Inada granite saturated with 0.001 mol/L (circles) and 0.01 mol/L (squares) KCl solutions. Also shown are theoretical values based upon Eqn. 4.

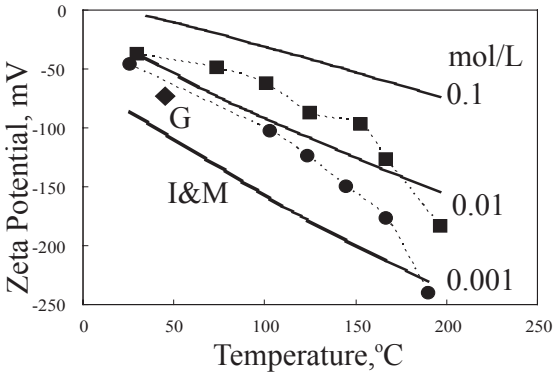

Figure 3. The ζ potential of Inada granite saturated with 0.001 mol/L (circles) and 0.01 mol/L (squares) KCl solutions. The ζ value measured previously for granular Inada granite is indicated by "G". Also shown are theoretical curves for quartz/NaCl solution system (Ishido and Mizutani, 1981).

with:

$$\mathbf{I_f} = [\varepsilon\zeta\eta R_{ev} G(\nabla P - \rho\mathbf{g})/\tau\,\mu]_f \times \psi \qquad (11)$$

$$\mathbf{I_m} = [\varepsilon\zeta\eta R_{ev} G(\nabla P - \rho\mathbf{g})/\tau\,\mu]_m \times (1-\psi) \qquad (12)$$

where:

$\mathbf{I_{total}}$ = total drag current density vector,
$\mathbf{I_f}$ = drag current density due to fracture zone effects,
$\mathbf{I_m}$ = drag current density due to matrix region effects,
ψ = fracture zone volume / total volume,
P = liquid-phase pressure,
ρ = liquid-phase mass density,
$\mathbf{g}$ = acceleration of gravity,

and where subscript "f" denotes conditions in the fracture zone, and subscript "m" denotes *"averaged"* conditions in the matrix region.

The EKP postprocessor computes the "fracture zone" drag current based on the liquid-phase mass flux in the fracture zone ($\mathbf{M_f}$) using Darcy's law:

$$\mathbf{M_f} = [Rk\rho\,(\rho\mathbf{g} - \nabla P)/\mu]_f \qquad (13)$$

so that:

$$\mathbf{I_f} = -\psi\,[\mathbf{M}\varepsilon\zeta\eta\,(R_{ev}/R)G/(\rho\tau k)]_f \qquad (14)$$

where "R" is liquid-phase relative permeability and the quantities within the brackets refer to conditions in the fracture zone. $\mathbf{M_f}$ is obtained directly from STAR's *"GEO"* output file. Although the average mass flux in the matrix region ($\mathbf{M_m}$) can be assumed to be negligible compared to $\mathbf{M_f}$, i.e. $|\mathbf{M_f}| >> |\mathbf{M_m}|$, $k_f >> k_m$ as well, so that the quantities $(\mathbf{M}/k)_f$ and $(\mathbf{M}/k)_m$ can be comparable in magnitude.

In the present model, the value of $\mathbf{I_{total}}$ is assumed to be expressable as:

$$\mathbf{I_{total}} = \mathbf{I_f}\,[1 + (\mathbf{I_m}/\mathbf{I_f})] \approx \mathbf{I_f}\,(1 + F) \qquad (15)$$

where $\mathbf{I_f}$ is calculated using Eqn. (14), and where the scalar factor F is given by:

$$F = B \times V \times D \qquad (16)$$

with:

$$B = [(R_{ev}/S)_m/(R_{ev}/S)_f] \times [(\varepsilon\zeta G/\tau\mu)_m/(\varepsilon\zeta G/\tau\mu)_f] \qquad (17)$$

$$V = (1-\psi)\,\eta_m\,S_m / \psi\,\eta_f\,S_f \qquad (18)$$

$$D = [(\nabla P - \rho\mathbf{g})_m / (\nabla P - \rho\mathbf{g})_f] \qquad (19)$$

In the above equations, "S" denotes liquid-phase saturation, in either the "fracture zone" (S_f) or the "matrix region" (S_m). Note that "B" is typically of order unity, "V" is simply the ratio of the liquid volume in the matrix region to that in the fracture zone, and "D" (the ratio of pressure gradients) will usually lie between zero and unity. The factor B is approximated as a user-prescribed unchanging function of position ("formation type") in the present version of the postprocessor. Note that, if B = 1 everywhere, under steady-state single-phase liquid conditions the drag current density calculated in this way is identical to that for an equivalent porous medium.

To calculate the grid-block-face drag current density within the RSV-grid, ψ, η, τ, k, G and ζ in (14) and B, V in (16) are computed at grid block interfaces using harmonic means. Other interface quantities in (14) are treated using a second-order upstream weighting scheme.

In view of the approximate nature of the present model, a few extra "special" rules are also imposed to avoid degenerate cases. First, it is necessary that the ratio (I_{total}/I_f) be non-negative to avoid destabilizing the numerical scheme. So, although the drag current in the matrix region can flow in the opposite direction to that in the fracture zone, the amplitude is restricted to values which will not change the sign of the net drag current. It is also required that the user-prescribed spatial function "B" be non-negative (the "default" value is unity).

"SP TRANSIENT" SIMULATION

2D Model

First, a pressure-transient simulation was performed for a two-dimensional horizontal reservoir model. The formation is represented by a "MINC" double-porosity medium with the following properties:

global permeability: $k = 10^{-14}$ m^2,
fracture zone volume fraction: $\psi = 0.1$,
fracture zone porosity: $\eta_f = 0.1$,
matrix region porosity: $\eta_m = 0.1$,
matrix region permeability: $k_m = 10^{-17}$ m^2,
fracture spacing: three values are considered:
λ = 10, 30 and 100 m,

The time required ($\tau_{pe} = \eta_m\,\mu\,C\lambda^2/10\,k_m$) for pressure equilibration between the fracture and matrix regions is ~10^4, ~10^5 and ~10^6 sec forλ = 10, 30 and 100 m, respectively. The initial thermodynamic state is uniform (temperature = 200°C and pressure = 10 MPa).

Between $0 \le t \le 0.3$ day, 200°C water is injected into the reservoir at 5 tons per hour per meter of reservoir thickness. Figure 4 shows the computed pressure interference signal 85 meters away from the injection point. Pressure signals do not reach the reservoir boundaries until t > 1 day. As Figure 4 indicates, for λ=30 and 100 m the pressure changes are larger in magnitude than for the λ=10 m and porous-equivalent (λ=0) cases. This is because pressure equilibrium between the fractures and the matrix region is not attained within one day for the larger fracture spacings.

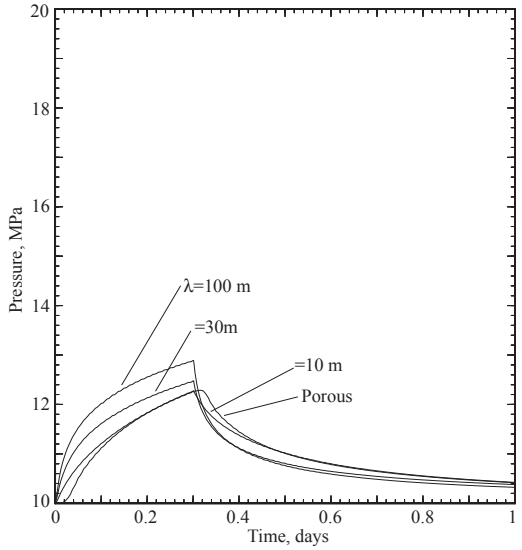

Figure 4. 2D model: pressure changes 85 m from the injection point for three values of fracture spacing and for the equivalent porous medium.

For the corresponding SP calculations, the reservoir fluid's NaCl concentration is assumed to be 0.002 mol/L, and the formation conductivity L_{ee} is constant at 0.003 S/m. The tortuosities are assumed to be 1 (τ_f=1) and 3.16 (τ_m=10) for the fractures and the matrix region respectively.

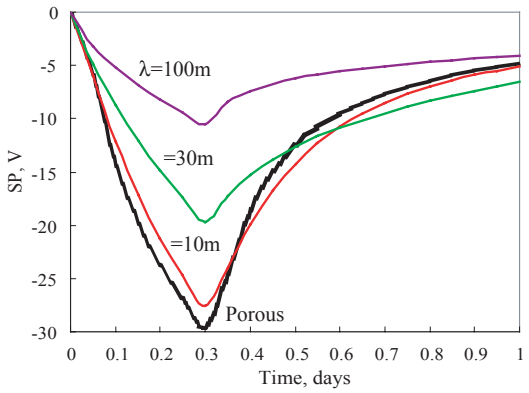

Figure 5. 2D model: Changes in SP 85 m from the injection point for three values of fracture spacing and for the equivalent porous medium.

Figure 5 shows the "SP transients" calculated by the EKP-postprocessor for the same four cases. In contrast to the pressure transients, the temporal SP changes are suppressed for larger fracture spacings. This is because the contribution of drag current through the matrix region is small at early times ($t << \tau_{pe}$). This property of the drag current is responsible for much more pronounced differences in the "SP transients" between competing "fractured/MINC" and "porous-medium" descriptions of the same reservoir than is the case for pressure transients.

Figure 6 shows semi-log plots of changes in pressure and in SP due to continuous injection at 0.5 tons per hour per meter of reservoir thickness. (Axi-symmetric coordinates with fine grid spacing near the injection well was adopted in this calculation.) The pressure transient at a point near the injection well shows behavior typical of a double-porosity medium: the late-time slope develops after the time required for pressure equilibrium within the matrix region τ_{pe} has elapsed.

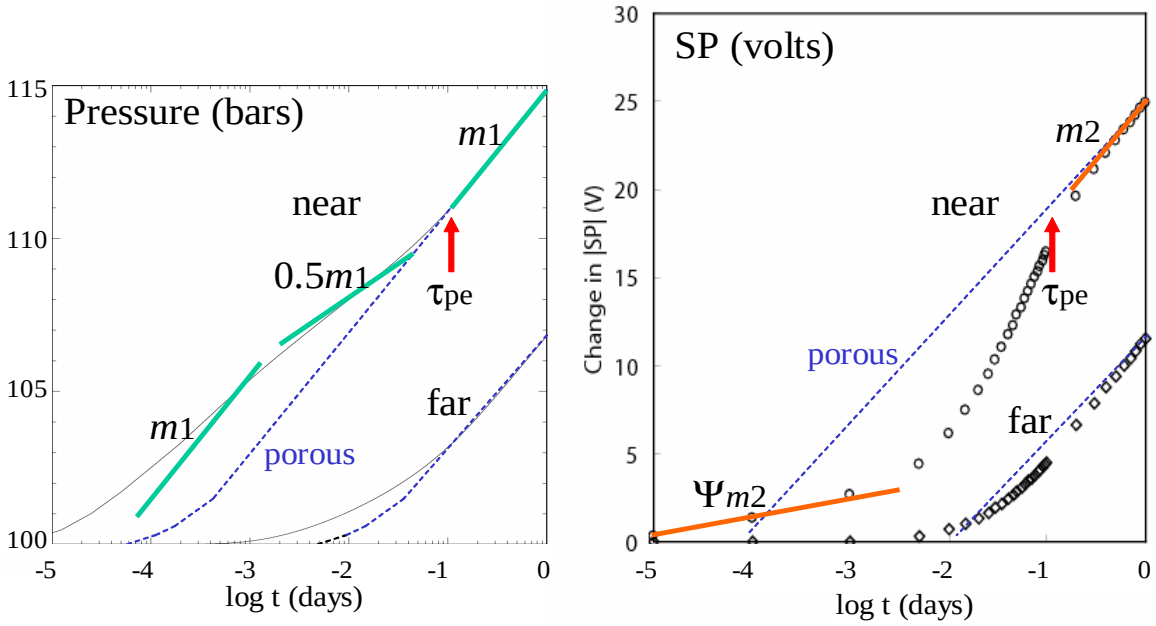

Figure 6. 2D axisymmetric model: Changes in pressure and SP for fractured medium with λ=10 m. The results for the equivalent porous medium are shown by broken curves. Labels "near" and "far" indicate that the observation point is ~5 m and ~50 m away from the injection well respectively.

The SP transient also shows three segments. The drag current contribution through the matrix region is small at early times, so the slope is smaller than that at late times, by the factor ψ (= 0.1). At intermediate times, the SP changes rapidly with increasing involvement of matrix region. The time τ_{pe} can be clearly identified at the intersection of the intermediate-time and late-time semi-log straight lines.

3D Model

Next, we consider a three-dimensional case with a horizontal fractured reservoir formation (10 m thick), which has the same properties and initial conditions as for the above 2D model. The reservoir layer is sandwiched by low-permeability (porous medium) host rocks, which have the same properties as those of the matrix region alone.

Figure 7 shows the pressure transients induced by 50 ton/hr, 200°C water injection (between t = 0 and 0.3 day). Large pressure changes occur within the fractured reservoir, but although gradual pressure changes are seen at the Z=20 m level in the host rock (15 m vertically from the boundary between the host rock and the fractured formation), no pressure changes have appeared deeper within the host rock by t = one day.

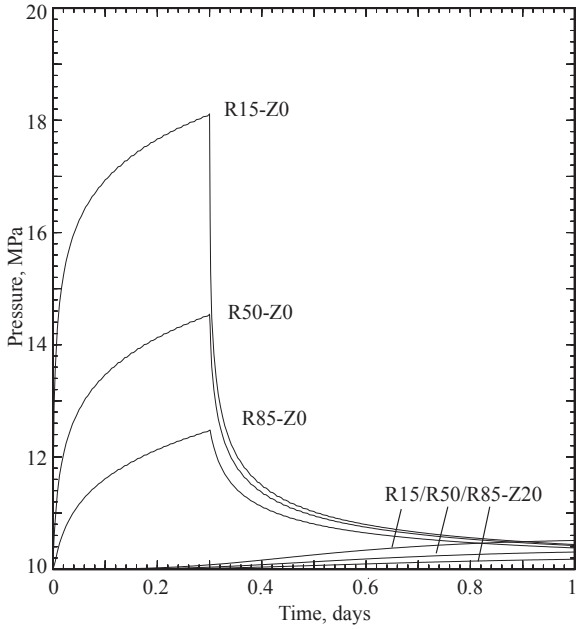

Figure 7. 3D model: changes in pressure for λ=30 m case. Labels attached to each curves indicate the location of observation points referred to the injection point; e.g. "R50-Z20" means that the point is located 50 m horizontally and 20 m vertically away from the injection point.

Figures 8a and 8b show the SP transients corresponding to the pressure transients shown in Figure 7. It is noteworthy that substantial SP signals appear at the Z= 20 and 100 m levels, where no significant pressure changes are observed. This behavior is brought about by the heterogeneity in the distribution of streaming potential coefficient C. (In the "equivalent porous medium" case, if C is the same in the permeable reservoir formation and the impermeable host rock, no SP signal will appear at points where no pressure change occurs.)

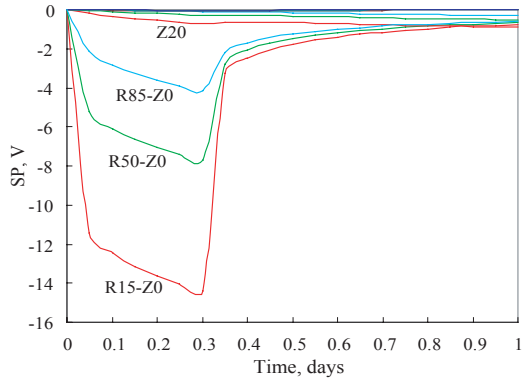

Figure 8a. 3D model: changes in SP for λ=30 m case.

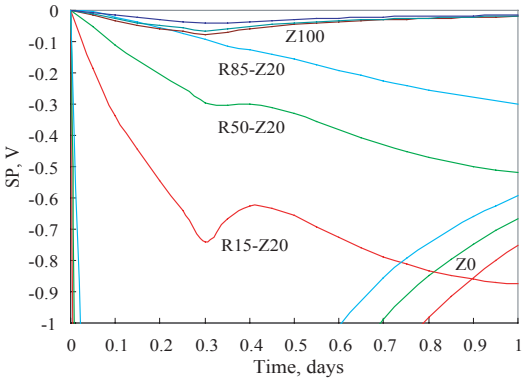

Figure 8b. 3D model: changes in SP for λ=30 m case (vertical axis expanded).

Furthermore, the calculated SP transients at Z= 20 and 100 m are detectable in practice, in contrast to the pressure changes. Even if the signals were only one-tenth of the present values (due to lower injection rate or higher reservoir permeability), the SP changes at Z =100 m would still be several millivolts, still large enough to be detected and characterized, in view of the quiet electrical conditions within a shut-in borehole (as shown in the next section).

It should be noted that SP signal appears even if the pressure disturbance does not reach the observation point in the host rocks. This remote-propagation of the SP signal is caused by the difference of the

streaming potential coefficient between the reservoir and the host rocks.

In this calculation, the square of tortuosity was assumed to be equal to unity for the fracture zone and equal to ten for the matrix region and the host rock. If we assume other tortuosity values (i.e., t^2 = 10 everywhere, including the fracture zone) the SP signals become quite different, as shown in Figure 9. The streaming potential coefficient C is time-dependent for double-porosity media, which necessarily causes a time-dependent C-contrast between the reservoir and host rocks. So, SP change at remote points in the host rocks is always to be expected, and the SP change pattern will depend on fracture parameters such as τ_{pe}, ψ and the porosity and tortuosity of the fracture and matrix regions.

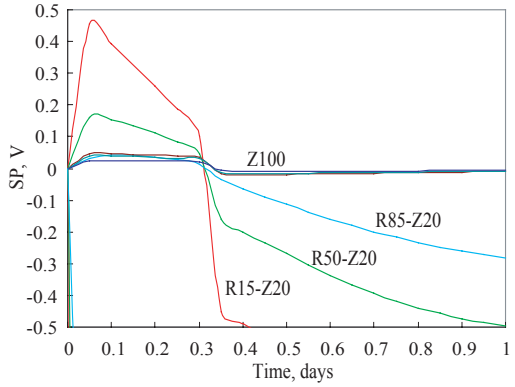

Figure 9. 3D model: SP changes for λ=30 m case, with tortuosity taken as t^2 =10 everywhere, in contrast to the case shown in Figure 8, in which t^2 =1 for the fracture zone and =10 for the matrix region and host rock.

DOWNHOLE SP MONITORING

In November 2001, sinusoidally modulated injection test experiments were carried out using two shallow (100 m) test wells, 30 meters apart, in the Sumikawa geothermal field (northern Japan). Figure 10 shows the results of continuous downhole SP monitoring using a SP-sonde equipped with two Ag-AgCl electrodes (both traces are shown) set at 75 meters depth in the open-hole interval (30-100 m) of well Gsk-2.

The most pronounced disturbance occurred when water was injected into well Gsk-2 itself, but note that a significant SP disturbance was also observed earlier in Gsk-2, when water was injected into nearby well Gsk-1. As these results show, the noise level is very low (~0.2 mV), in contrast to very large (artificial) electrical noise levels at the ground surface near the wellhead. The pressure interference signal observed in well Gsk-2 due to injection into Gsk-1 was not clear enough for quantitative analysis. But the "SP interference" signal was far above the noise level, even though we cannot distinguish the individual peaks corresponding to the sinusoidal injection maxima (owing to the coarse ten-minute recording interval that was employed for long term SP monitoring in well Gsk-2).

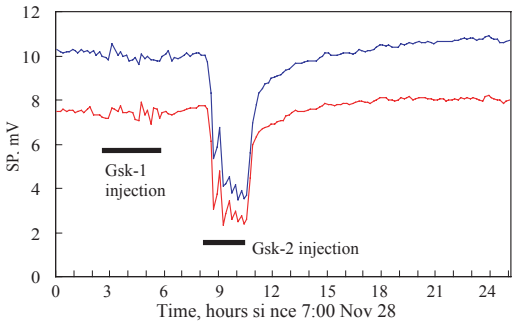

Figure 10. Changes in downhole SP observed in well Gsk-2 relative to a surface electrode located far away from the noise sources at the drilling pad (Ishido et al., 2003).

CONCLUDING REMARKS

Downhole SP monitoring appears to have a great deal of promise for complementing pressure transient data to help map and characterize fracture networks. Although high temperature downhole instrumentation for SP measurements poses greater challenges than conventional earth-surface surveys, the noise level (caused by both cultural and meteorological phenomena) that limits surface survey precision is much less troublesome at depth.

The present calculation suggests that SP signals of hundreds of millivolts amplitude should be observable on time-scales of a few days or less even at considerable distances (tens of meters) from the fracture zone. Signals of this strength vastly exceed practical detection thresholds for downhole SP measurements.

REFERENCES

Corwin, R.F. and Hoover, D.B. (1979), "The Self-potential Method in Geothermal Exploration," *Geophysics*, **44**, 226-245.

Ishido, T. (1989), "Self-potential Generation by Subsurface Water Flow Through Electrokinetic Coupling," in *Detection of Subsurface Flow Phenomena*, *Lecture Notes in Earth Sciences*, Vol. 27, edited by G.-P. Merkler et al., pp.121-131, Springer-Verlag, Berlin.

Ishido, T., Kikuchi, T. and Sugihara, M. (1987), "The Electrokinetic Mechanism of Hydrothermal-

circulation-related and Production-induced Self Potentials," *Proc.12th Stanford Workshop on Geothermal Reservoir Engineering*, 285-290.

Ishido, T. and Mizutani, H. (1981), "Experimental and Theoretical Basis of Electrokinetic Phenomena in Rock-water Systems and its Applications to Geophysics," *Journal of Geophysical Research*, **86**, 1763-1775.

Ishido, T, Nakao, S. and Kikuchi, T. (2003), "Downhole SP monitoring During the Injection Tests of Wells Gsk-1 and -2," *GSJ Interim Report*.

Ishido, T., and Pritchett, J.W. (1996), "Numerical Simulation of Electrokinetic Potentials Associated with Subsurface Fluid Flow," *Proc. 21st Stanford Workshop on Geothermal Reservoir Engineering*, 143-149.

Ishido, T., and Pritchett, J.W. (1999), "Numerical Simulation of Electrokinetic Potentials Associated with Subsurface Fluid Flow," *Journal of Geophysical Research*, **104**, 15,247-15,259.

Jouniaux, L. and Pozzi, J.-P. (1995), "Permeability Dependence of Streaming Potential in Rocks for various Fluid Conductivities," *Geophysical Research Letters*, **22**, 485-488.

Pritchett, J.W. (1995), "STAR: A Geothermal Reservoir Simulation System," *Proc. World Geothermal Congress*, 2959-2963, IGA, Florence.

Pruess, K. and Narasimhan, T.N. (1982), "A Practical Method for Modeling Fluid and Heat Flow in Fractured Porous Media", presented at the Reservoir Simulation Symposium of the Society of Petroleum Engineers, New Orleans, Louisiana, Jan. 31 - Feb. 3 (Also see SPE Journal, Feb. 1985, pp.14-26).

Tosha, T., Matsushima, N. and Ishido, T. (2003), "Zeta Potential Measured for an Intact Granite Sample at Temperatures to 200°C," *Geophysical Research Letters* (in press).

Zablocki, C.J. (1976), "Mapping Thermal Anomalies on an Active Volcano by the Self-potential Method, Kilauea, Hawaii," *Proc. 2nd U.N. Symposium on the Development and Use of Geothermal Resources*, vol. 2, 1299-1309, San Francisco.

Zohdy, A.A.R., Anderson, L.A. and Muffler, L.J.P. (1973), "Resistivity, Self-potential, and Induced-polarization Surveys of a Vapor-dominated Geothermal System," *Geophysics*, **38**, 1130-1144.